DOI:
10.1063/1.5083924

Document Version
Publisher's PDF, also known as Version of record

Mean first passage times in variational coarse graining using Markov state models

Cite as: J. Chem. Phys. **150**, 134107 (2019); https://doi.org/10.1063/1.5083924
Submitted: 01 December 2018 . Accepted: 22 February 2019 . Published Online: 04 April 2019

Adam Kells, Zsuzsanna É. Mihálka, Alessia Annibale, and Edina Rosta

The Journal of Chemical Physics ARTICLE scitation.org/journal/jcp

Mean first passage times in variational coarse graining using Markov state models

Cite as: J. Chem. Phys. 150, 134107 (2019); doi: 10.1063/1.5083924
Submitted: 1 December 2018 • Accepted: 22 February 2019 •
Published Online: 4 April 2019

Adam Kells,[1] Zsuzsanna É. Mihálka,[2] Alessia Annibale,[3] and Edina Rosta[1,a)]

AFFILIATIONS

[1]Department of Chemistry, Kings College London, London, England
[2]Laboratory of Theoretical Chemistry, ELTE Eötvös Loránd University, Budapest, Hungary
[3]Department of Mathematics, Kings College London, London, England

Note: This article is part of the Special Topic "Markov Models of Molecular Kinetics" in J. Chem. Phys.
[a)]**Email:** edina.rosta@kcl.ac.uk

ABSTRACT

Markov state models (MSMs) provide some of the simplest mathematical and physical descriptions of dynamical and thermodynamical properties of complex systems. However, typically, the large dimensionality of biological systems studied makes them prohibitively expensive to work in fully Markovian regimes. In this case, coarse graining can be introduced to capture the key dynamical processes—slow degrees of the system—and reduce the dimension of the problem. Here, we introduce several possible options for such Markovian coarse graining, including previously commonly used choices: the local equilibrium and the Hummer Szabo approaches. We prove that the coarse grained lower dimensional MSM satisfies a variational principle with respect to its slowest relaxation time scale. This provides an excellent framework for optimal coarse graining, as previously demonstrated. Here, we show that such optimal coarse graining to two or three states has a simple physical interpretation in terms of mean first passage times and fluxes between the coarse grained states. The results are verified numerically using both analytic test potentials and data from explicit solvent molecular dynamics simulations of pentalanine. This approach of optimizing and interpreting clustering protocols has broad applicability and can be used in time series analysis of large data.

I. INTRODUCTION

The emergence of Markov State Models (MSMs) as a formalism for analysing and interpreting equilibrium molecular dynamics (MD) simulation data in a statistically optimal manner has proven to be one of the most important recent developments in the field of computational chemistry (for details of MSM methods, see recent reviews[6–9] and applications[1–5,10]).

In particular, MSMs are used by academia as well as the pharmaceutical industry to identify clusters of metastable states from multiple short unbiased MD simulations, providing a useful stepping stone for subsequent drug discovery in many cases.[11–13]

A particular advantage of an MSM analysis over standard thermodynamic clustering is that the kinetic rates of key underlying processes are possible to calculate, leading to better understanding of complex systems. This MSM analysis allows for quantitative comparison and prediction of important experimental data, such as relaxation time scales,[14] protein-ligand un/binding rates,[15–17] membrane crossing times,[13,18] and many more.

Recent developments enable MSM analysis of enhanced sampling simulation data, including replica exchange simulations[19] and umbrella sampling biased simulation data.[20–22] MSMs bridge a gap, enabling access to long time scales only obtainable via enhanced sampling algorithms.

Of particular interest in this work is the identification of metastable[3,23] and transition states[24] in an optimal manner. This has been one of the key questions since the seminal work of Zwanzig[25] as dimensionality increases exponentially with the number of degrees of freedom, making a fully Markovian description unfeasible for complex biological systems. By examining the effects of projecting classical dynamics onto clustered coarse-grained states, Zwanzig developed a short-memory approximation to the time-dependent rate matrix. With appropriately chosen clustered states, the full microscopic dynamics can be considered "sufficiently

complex" that the system does not retain memory of reaching its current coarse-grained state and one can obtain a simple expression for Markovian transition rates between the clustered system states.

Dimensionality reduction however necessarily comes together with loss of information. It is a key question to identify how to minimize this loss, and this will depend on the definition of the clusters and furthermore on the definition of the kinetics on the reduced clusters. Traditionally, most clustering approaches are built on the idea that dynamics within clusters should be fast, while dynamics between clusters should be slow and use the spectral properties of the Markov transition matrix (eigenvalues/vectors) to identify the most stable states.[26–32] Other early approaches used the concept of likelihood maximization for model dimensionality reduction.[33,34] These approaches have proven effective at identifying metastable states.

In recent years, there have been several new more complex dynamics-based algorithms developed using, e.g., Bayesian inference[35,36] or the "most probable path" algorithm.[37,38] These new approaches are designed to identify poorly sampled or unstable microstates and coarse grain them to their most stable basin. However, these methods similarly focus on identifying metastable states.

To also identify key transition states in addition to metastable states optimally in the context of MSMs, we previously described a procedure[24] based on the Hummer-Szabo (HS) clustering approach.[39] This approach enforces that the slow dynamics of the system are made as slow as possible. As this requirement is less restrictive than making interstate dynamics slower than intrastate dynamics, it allows for short-lived transition states to be identified. This method is based on the idea of optimizing the coarse-grained Markov matrix eigenvalues, which was also used by Schütte, Noé, and co-workers in the context of quantifying discretization effects and proving a variational upper limit on the error of the second eigenvalue.[40–42]

Here, we propose alternative options for possible definitions to obtain Markovian coarse-grained systems, including as special cases the Hummer-Szabo and local equilibrium definitions. Intuitively, the slowest time scale of the reduced MSM is faster than that of the original MSM. This has been shown for general self-adjoint operators with specific normalization properties using the analogy to the Rayleigh-Ritz linear variational method in quantum chemistry[43,44] and applied to approximate exact MSMs optimally using a set of basis functions.[44] Here, we prove that such a variational principle with respect to the eigenvalues of the MSMs applies to the coarse-graining methods that we present. We provide two different proofs: first, a simple intuitive derivation (illustrated for the Hummer-Szabo definition in the main text and for the local equilibrium in the Appendix C) and second, constructing a non-trivial operator and applying the Rayleigh-Ritz method.

Furthermore, we provide an intuitive description assuming equilibrium diffusive dynamics for the optimally clustered states, which arise from following the procedures described above. To do this, the dimensionality reduction method is expressed in terms of correlation functions and in turn these correlation functions are expressed as mean first passage times (MFPTs) between clustered states.

The simple physical expressions that arise are verified on both analytic free energy profiles and MD simulation data of pentalanine in explicit water. Furthermore, a range of clustering protocols are compared and contrasted for the different test cases. Finally, we provide a discussion on the general applicability of this method and possible future directions by which it might be expanded upon.

II. THEORY

A. Markov state model

An MSM is used to model the dynamics of a system as a memoryless process such that the next state of the system depends only on its present state. Constructing MSMs in practice involves defining a discrete set of states which the system can occupy. These states are labeled by $i, j, \ldots$, where $i, j \in [1, 2, \ldots, n]$ (n is the dimensionality of the system). A set of transition rates k_{ji} (in units of inverse time) can be defined between the states, as the number of transitions per unit time from state i to j divided the number of transitions out of state i.

The probability of occupation of a state j at time t, $p_j(t)$, is then found by solving the master equation, which relates the rate of change in the probability, to the difference between the flux into and out of the state

$$\frac{dp_j(t)}{dt} = \sum_{i \neq j} \left[k_{ji} p_i(t) - k_{ij} p_j(t) \right], \tag{1}$$

or, in the matrix form, using the property of rate matrices, $\sum_i k_{ij} = 0$,

$$\frac{d\mathbf{p}}{dt} = \mathbf{K}\mathbf{p}. \tag{2}$$

We denote with $\mathbf{p}^{\mathrm{eq}}$ the stationary solution and we will assume that it satisfies detailed balance with the transition rates, i.e., $k_{ji} p_i^{\mathrm{eq}} = k_{ij} p_j^{\mathrm{eq}} \ \forall \ i, j$, so that the stationary state is equilibrium. The time-dependent solution is found in exponential form $\mathbf{p}(t) = e^{\mathbf{K}t}\mathbf{p}(0)$, where $e^{\mathbf{K}t}$ is the propagator, whose entries $[e^{\mathbf{K}t}]_{ij} = P(i, t|j, 0)$ give the probability to find the system in a state i at a time t, given its state is j at time zero. The nature of the analysis in Sec. II D requires to work in Laplace space and transform the time variable t into a Laplace variable s. A Laplace transform is defined as $\hat{\mathbf{F}}(s) = \int_0^\infty f(t) e^{-st} dt$ for any function of time $f(t)$. Performing a Laplace transform to both sides of the master equation

$$s\hat{\mathbf{p}}(s) - \mathbf{p}(0) = \mathbf{K}\hat{\mathbf{p}}(s) \tag{3}$$

has the useful effect of replacing the differential master equation with a purely algebraic equation.

B. Spectral properties of rate matrices

In order to extract information about the system from the Markovian rate matrix, it is necessary to examine the eigenvalues and eigenvectors of the matrix.

For a system containing n possible states, the rate matrix describing the transition rates will be of dimension $n \times n$ and it will have n eigenvalues and n eigenvectors of length n, defined by

$$\mathbf{K}\Psi_k^R = \lambda_k \Psi_k^R. \tag{4}$$

Here, Ψ_k^R denotes the kth right eigenvector of the matrix and similarly Ψ_k^L will denote the kth left eigenvector. There will be a zero eigenvalue with a corresponding left eigenvector $\mathbf{1}_n^T = (1, \ldots, 1)$ with n components equal to one and the right eigenvector giving (when normalized such that $\Psi_k^L \cdot \Psi_\ell^R = \delta_{k\ell}$) the equilibrium probability $\mathbf{p}^{\mathrm{eq}} = (p_1^{\mathrm{eq}}, \ldots, p_n^{\mathrm{eq}})^T$ for each of the n states. The remaining $n-1$ eigenvalues are all negative ($0 = \lambda_1 > \lambda_2 \geq \cdots \geq \lambda_n$) and are inversely related to the time scales τ_k within the system

$$\tau_k = -\frac{1}{\lambda_k}. \tag{5}$$

The signs of the elements of Ψ_k^R give the clustered states on which the corresponding time scale τ_k occurs.[45] This is the basis of many existing methods for performing clustering using the rate matrix eigenvectors.[28]

C. Correlation functions

In many studies of dynamical systems, the connected correlator between two observables θ_i and θ_j

$$C_{ij}(\tau, t) = \langle \theta_i(t+\tau)\theta_j(t)\rangle - \langle \theta_i(\tau+t)\rangle\langle \theta_j(t)\rangle \tag{6}$$

arises as a useful quantity to analyse. This gives the correlation between the two observables measured at a time separation τ, and it satisfies, in equilibrium, the fluctuation-dissipation relation.[46,47] In the correlator equation (6), the average $\langle\cdot\rangle = \sum_{xx'} \cdot P(x, t+\tau|x', t)$ is taken over the probabilities of all dynamical paths between configurations x' and x, sampled at time t and $t+\tau$, respectively. A convenient observable to probe correlations is the occupancy-number

$$\theta_i(t) = \begin{cases} 1 & x(t) = i \\ 0 & \text{otherwise'} \end{cases} \tag{7}$$

an indicator function which signals the state $i \in [1, 2, \ldots, n]$ in which the system is found at any given time, where $x(t)$ denotes a discrete reaction coordinate (or discretised via a binning procedure) that describes the system. The correlator is then directly related to the propagator via

$$C_{ij}(\tau, t) = [e^{\mathbf{K}\tau}]_{ij} p_j(t) - p_i(t+\tau)p_j(t). \tag{8}$$

Averaging over t and assuming ergodicity of trajectories, this becomes a function of the time difference τ only

$$\tilde{C}_{ij}(\tau) = [e^{\mathbf{K}\tau}]_{ij} p_j^{\mathrm{eq}} - p_i^{\mathrm{eq}} p_j^{\mathrm{eq}}, \tag{9}$$

which we can write in matrix notation as

$$\tilde{\mathbf{C}}(\tau) = [e^{\mathbf{K}\tau}]\mathbf{D}_n - \mathbf{D}_n\mathbf{D}_n^T, \tag{10}$$

where $\mathbf{D}_n$ is the diagonal matrix with $\mathbf{p}^{\mathrm{eq}}$ along its diagonal, i.e., with entries $(\mathbf{D}_n)_{ij} = p_i^{\mathrm{eq}}\delta_{ij}$. Taking the Laplace transform, we have

$$\hat{\tilde{\mathbf{C}}}(s) = (s\mathbf{I}_n - \mathbf{K})^{-1}\mathbf{D}_n - \frac{1}{s}\mathbf{D}_n\mathbf{D}_n^T, \tag{11}$$

where $(s\mathbf{I}_n - \mathbf{K})^{-1}$ is the propagator in Laplace space. There have been many studies examining the usefulness and properties of these quantities, in particular, how they relate to mean first passage times (MFPTs) between states.[48–50] The key results from the referenced studies will be taken advantage of to provide intuitive interpretations of the results in Sec. III C.

D. Constructing a dimensionally reduced rate matrix

In this subsection, we show how the projection operator formalism can be used to perform a correlation function based clustering.

Suppose that a projection operator $\mathcal{P}$ is used to project microstates down on to some sub-space. We denote $\mathbf{u} = \mathcal{P}\mathbf{p}$ the projected probability vector and $\mathbf{v} = \mathbf{p} - \mathbf{u}$ its orthogonal projection $\mathbf{v} = \mathcal{Q}\mathbf{p}$, with $\mathcal{Q} = \mathbf{I}_n - \mathcal{P}$ and $\mathbf{I}_n$ is the n-dimensional identity matrix. From Eq. (2), a pair of coupled differential equations for the projections of $\mathbf{p}$ can be obtained

$$\frac{d\mathbf{u}}{dt} = \mathcal{P}\mathbf{K}\mathbf{u} + \mathcal{P}\mathbf{K}\mathbf{v}, \tag{12}$$

$$\frac{d\mathbf{v}}{dt} = \mathcal{Q}\mathbf{K}\mathbf{u} + \mathcal{Q}\mathbf{K}\mathbf{v}. \tag{13}$$

Solving the equation for $\mathbf{v}$, with initial condition $\mathbf{v}(0) = 0$, and substituting into the equation for $\mathbf{u}$ lead to a dynamical description involving only $\mathbf{u}$

$$\frac{d\mathbf{u}}{dt} = \int_0^t \mathbf{M}(t-\tau)\mathbf{u}(\tau)d\tau, \tag{14}$$

which is no longer Markovian, where

$$\mathbf{M}(t-\tau) = \mathcal{P}\mathbf{K}\delta(t-\tau) + \mathcal{P}\mathbf{K}e^{\mathcal{Q}\mathbf{K}(t-\tau)}\mathcal{Q}\mathbf{K} \tag{15}$$

is a memory kernel encoding the effective interaction between $\mathbf{u}$ and its past values, arising from interactions with the degrees of freedom that have been integrated out.

Suppose we want to cluster the microstates $i \in \{1, \ldots, n\}$ into $N < n$ macrostates, which we label with capital indices $I, J \in \{1, \ldots, N\}$. We define $\mathbf{P}$ the probabilities on the macrostates, which are related to $\mathbf{p}$ via $\mathbf{P} = \mathbf{A}^T\mathbf{p}$, where $\mathbf{A}$ is an $n \times N$ aggregation matrix with entries A_{iI} equal to 1 if microstate $i \in I$ and zero otherwise. The macrostate probabilities evolve according to a memory kernel equation

$$\frac{d\mathbf{P}}{dt} = \int_0^t \mathbf{R}(t-\tau)\mathbf{P}(\tau)d\tau. \tag{16}$$

Laplace transforming as in Eq. (3) and rearranging

$$\hat{\mathbf{P}}(s) = (s\mathbf{I}_N - \hat{\mathbf{R}}(s))^{-1}\mathbf{P}(0) \tag{17}$$

give the propagator $(s\mathbf{I}_N - \hat{\mathbf{R}}(s))^{-1}$ in Laplace space, which can be used to express the correlator of the coarse-grained system

$$\hat{\tilde{\mathbf{C}}}^{\mathrm{CG}}(s) = (s\mathbf{I}_N - \hat{\mathbf{R}}(s))^{-1}\mathbf{D}_N - \frac{1}{s}\mathbf{D}_N\mathbf{D}_N^T. \tag{18}$$

Here, $\mathbf{D}_N$ is the diagonal matrix with the stationary solution of Eq. (16) $\mathbf{P}^{\mathrm{eq}}$ on the diagonal.

Two key questions are which projection corresponds to the clustering protocol $\mathbf{A}$ and how the rate matrix of the coarse-grained system $\hat{\mathbf{R}}(s)$ is related to the one of the original system $\mathbf{K}$. Defining the relation between $\mathbf{u}$ and $\mathbf{P}$ to be described by an $n \times N$ matrix $\mathbf{H}$ such that $\mathbf{u} = \mathbf{H}\mathbf{P}$, one has from $\mathbf{u} = \mathcal{P}\mathbf{p}$ and $\mathbf{P} = \mathbf{A}^T\mathbf{p}$ that $\mathcal{P} = \mathbf{H}\mathbf{A}^T$.

The condition that $\mathcal{P}^2 = \mathcal{P}$ (necessary for a projection operator) yields $\mathbf{A}^T\mathbf{H} = \mathbf{I}_N$. Using this relation and combining Eq. (17) with the Laplace transform of Eq. (14)

$$s\hat{\mathbf{u}}(s) - \mathbf{u}(0) = \hat{\mathbf{M}}(s)\hat{\mathbf{u}}(s) \tag{19}$$

give $\hat{\mathbf{R}}(s) = \mathbf{A}^T\hat{\mathbf{M}}(s)\mathbf{H}$ from which, Laplace transforming (15), we obtain

$$\hat{\mathbf{R}}(s) = s\mathbf{A}^T\mathbf{K}(s\mathbf{I}_n - \mathbf{K} + \mathbf{H}\mathbf{A}^T\mathbf{K})^{-1}\mathbf{H}. \tag{20}$$

$\mathbf{H}$ must be chosen to ensure that the stationary solution of (16) is $\mathbf{P}^{\mathrm{eq}} = \mathbf{A}^T\mathbf{p}^{\mathrm{eq}}$. This choice is not unique; however, a sufficient condition is that $\mathbf{P}^{\mathrm{eq}}$ satisfies detailed balance with $\hat{\mathbf{R}}(s)$ for all s, i.e.,

$$\hat{\mathbf{R}}(s)\mathbf{D}_N = \mathbf{D}_N\hat{\mathbf{R}}^T(s).$$

We show in Appendix A that the choice

$$\mathbf{H} = \mathbf{D}_n\mathbf{A}\mathbf{D}_N^{-1} \tag{21}$$

fulfills this requirement for all s. This can be easily checked for the limit $s \to \infty$, where (20) evaluates to

$$\hat{\mathbf{R}}(\infty) = \mathbf{A}^T\mathbf{K}\mathbf{H}$$

and substituting (21) gives

$$\hat{\mathbf{R}}(\infty)\mathbf{D}_N = \mathbf{A}^T\mathbf{K}\mathbf{D}_n\mathbf{A}.$$

This is equal to $\mathbf{D}_N\hat{\mathbf{R}}^T(\infty)$ as long as the rate matrix of the original system $\mathbf{K}$ satisfies detailed balance with $\mathbf{p}^{\mathrm{eq}}$, i.e., $\mathbf{K}\mathbf{D}_n = \mathbf{D}_n\mathbf{K}^T$. From now on, we will restrict to choice (21), which preserves the detailed balance condition assumed in the original system, thus making the coarse-grained dynamics equilibrium. Generalizations to dynamics which are originally non-equilibrium, or to dimensionality reductions that break the detailed balance of originally equilibrium systems, will constitute an interesting pathway for future research. For the choice (21),

$$\mathcal{P} = \mathbf{D}_n\mathbf{A}\mathbf{D}_N^{-1}\mathbf{A}^T \tag{22}$$

and $\mathbf{u}_i(t) = [\mathbf{p}_i^{eq}\mathbf{P}_I(t)]/\mathbf{P}_I^{eq}$, $\forall\, i \in I$, so that the elements of $\mathbf{u}$ tend to the same limit as the elements of $\mathbf{p}$. Substituted into Eq. (20), this choice for $\mathbf{H}$ gives the relation first obtained in Ref. 39

$$\hat{\mathbf{R}}(s) = s\mathbf{A}^T\mathbf{K}(s\mathbf{I}_n - \mathbf{K} + \mathbf{D}_n\mathbf{A}\mathbf{D}_N^{-1}\mathbf{A}^T\mathbf{K})^{-1}\mathbf{D}_n\mathbf{A}\mathbf{D}_N^{-1}, \tag{23}$$

which is remarkable in that it shows how to construct the rate matrix of a low-dimensional dynamics purely in terms of the rate matrix $\mathbf{K}$ of the original high-dimensional dynamics and a choice of clustering $\mathbf{A}$.

To obtain a physically intuitive interpretation of this result, Eq. (23) is rearranged to be of the same form as the Laplace transform of a correlation function, as in Eq. (11). This expression can be simplified down using the Woodbury inversion formula

$$(\mathbf{M} + \mathbf{U}\mathbf{V})^{-1} = \mathbf{M}^{-1} - \mathbf{M}^{-1}\mathbf{U}(\mathbf{I}_n + \mathbf{V}\mathbf{M}^{-1}\mathbf{U})\mathbf{V}\mathbf{M}^{-1} \tag{24}$$

and identifying $\mathbf{M} = (s\mathbf{I}_n - \mathbf{K})$, $\mathbf{U} = \mathbf{D}_n\mathbf{A}\mathbf{D}_N^{-1}$, and $\mathbf{V} = \mathbf{A}^T\mathbf{K}$. In simplifying down, it is useful to notice that $\mathbf{V}\mathbf{M}^{-1}\mathbf{U} = s\mathbf{A}^T\mathbf{M}^{-1}\mathbf{U} - \mathbf{I}_N$.

Using these two relations, it is straightforward to obtain the simpler result

$$\hat{\mathbf{R}}(s) = s\mathbf{I}_N - (\mathbf{A}^T(s\mathbf{I}_n - \mathbf{K})^{-1}\mathbf{D}_n\mathbf{A}\mathbf{D}_N^{-1})^{-1}. \tag{25}$$

This can be rearranged into the form

$$\mathbf{A}^T(s\mathbf{I}_n - \mathbf{K})^{-1}\mathbf{D}_n\mathbf{A} = (s\mathbf{I}_N - \hat{\mathbf{R}}(s))^{-1}\mathbf{D}_N. \tag{26}$$

Since $s^{-1}\mathbf{A}^T\mathbf{D}_n\mathbf{D}_n^T\mathbf{A} = s^{-1}\mathbf{D}_N\mathbf{D}_N^T$ can be subtracted from both sides, we have

$$\mathbf{A}^T\left((s\mathbf{I}_n - \mathbf{K})^{-1}\mathbf{D}_n - \frac{1}{s}\mathbf{D}_n\mathbf{D}_n^T\right)\mathbf{A} = \hat{\bar{\mathbf{C}}}^{CG}(s), \tag{27}$$

where we have used Eq. (18). Finally, using Eq. (11) leads to

$$\sum_{i\in I}\sum_{j\in J}\int_0^\infty \bar{C}_{ij}(t)e^{-st}dt = \int_0^\infty \bar{C}_{IJ}^{CG}(t)e^{-st}dt, \tag{28}$$

showing that the condition which arises naturally from attempting to reproduce the high dimensional kinetics on a low dimensional space is to equate Laplace transformed correlation functions.

III. RESULTS

A. Markovian coarse graining

In Sec. II D, the correlation element protocol arose naturally out of enforcing a projected dynamics to preserve detailed balance. Additionally, we aim to define a Markovian coarse grained system. This requires further approximations, in which Eq. (28) cannot be fully satisfied. Here, we define possible choices to arrive to a Markovian system that preserves some properties of the correlation functions of the original system. By ensuring that Eq. (28) is exact for the $s \to 0$ limit, we obtain the Hummer-Szabo definition

$$\sum_{i\in I}\sum_{j\in J}\int_0^\infty \bar{C}_{ij}(t)dt = \int_0^\infty \bar{C}_{IJ}^{CG}(t)dt. \tag{29}$$

In Secs. III B and III C, we will focus on this definition.

On the other hand, we can define the time integral of the correlation functions to be equal between two selected times, τ_1 and τ_2, for the coarse-grained and full dimensional dynamics

$$\sum_{i\in I}\sum_{j\in J}\int_{\tau_1}^{\tau_2} \bar{C}_{ij}(t)dt = \int_{\tau_1}^{\tau_2} \bar{C}_{IJ}^{CG}(t)dt. \tag{30}$$

This is a general new definition, and we show in Appendix B that a variational principle applies in this case as well.

As a special case, we can select a specific time $\tau_1 = \tau$ and set $\tau_2 = \tau + \epsilon$, where the limit $\epsilon \to 0$ is taken, for which the above condition gives

$$\sum_{i\in I}\sum_{j\in J}\bar{C}_{ij}(\tau) = \bar{C}_{IJ}^{CG}(\tau). \tag{31}$$

This choice corresponds to the typical construction of MSMs using a selected lagtime τ. We refer to this definition as the local equilibrium definition. In the specific choice of $\tau = 0$, we also obtain the limit of $s \to \infty$ for Eq. (28)

$$\sum_{i\in I}\sum_{j\in J}\bar{C}_{ij}(0) = \bar{C}_{IJ}^{CG}(0). \tag{32}$$

Alternative choices could also be considered by setting the Laplace variable s to a specific finite value.

B. Variational bound on the coarse-grained relaxation time

We demonstrate that the rate matrix obtained from the coarse graining in Sec. II D is variational in its second eigenvalue in a number of general cases. We leave the more general case to Appendix B and here demonstrate this for the Hummer-Szabo case as that will be of particular interest in Sec. III C.

The proof for the local equilibrium case with $\tau = 0$ is completely analogous and is provided in Appendix C. The proof offered in this section is an intuitive, element-wise approach. For completeness, a more formal proof demonstrating the variational principle for a time integral between some arbitrary times τ_1 and τ_2 is provided in Appendix B. This more general proof contains both the local equilibrium and Hummer-Szabo definitions as special cases.

Performing a spectral decomposition of the Hummer Szabo condition and using μ_n and $\mathbf{\Phi}_n^R$ to denote the n-th eigenvalue and eigenvector, respectively, in the reduced system

$$\int_0^\infty \sum_{n'=2}^{N} e^{\mu_{n'} t} \Phi_{n'}^R(I)\Phi_{n'}^R(J)dt = \sum_{i\in I}\sum_{j\in J}\int_0^\infty \sum_{n'=2}^{n} e^{\lambda_{n'} t}\psi_{n'}^R(i)\psi_{n'}^R(j)dt. \tag{33}$$

Next, time can be integrated on both sides

$$\sum_{n'=2}^{N}\frac{-1}{\mu_{n'}}\Phi_{n'}^R(I)\Phi_{n'}^R(J) = \sum_{i\in I}\sum_{j\in J}\sum_{n'=2}^{n}\frac{-1}{\lambda_{n'}}\psi_{n'}^R(i)\psi_{n'}^R(j). \tag{34}$$

Multiplying both sides by $\Phi_2^L(I)\Phi_2^L(J)$ and summing over all macrostates I and J, the second eigenvalue can be isolated

$$\frac{-1}{\mu_2} = \sum_{I,J}\sum_{i\in I}\sum_{j\in J}\sum_{n'=2}^{n}\frac{-1}{\lambda_{n'}}\psi_{n'}^R(i)\psi_{n'}^R(j)\Phi_2^L(I)\Phi_2^L(J). \tag{35}$$

Since I and J are indices that run over the same values,

$$\frac{-1}{\mu_2} = \sum_{n'=2}^{n}\frac{-1}{\lambda_{n'}}\left(\sum_I\sum_{i\in I}\psi_{n'}^R(i)\Phi_2^L(I)\right)^2 = \sum_{n'=2}^{n}\frac{-1}{\lambda_{n'}}a_{n'} \tag{36}$$

with the definitions $a_{n'} = (\sum_I \sum_{i\in I}\psi_{n'}^R(i)\Phi_2^L(I))^2$. From the orthogonality and normalization of the eigenvectors, it can be shown that $\sum_{n'=2}^{n} a_{n'} = 1$, giving

$$\frac{-1}{\mu_2} \le \frac{-1}{\lambda_2}\sum_{n'=2}^{n} a_{n'} = \frac{-1}{\lambda_2}. \tag{37}$$

Since the negative inverse of the eigenvalue is the relaxation time, the slowest relaxation time of the dimensionally reduced matrix $\mathbf{R}$ is always less than or equal to that of the original system $\mathbf{K}$

$$\tau_2^R \le \tau_2^K. \tag{38}$$

C. Optimal slowest coarse-grained relaxation times

In Sec. III B, we showed that the Hummer-Szabo method for obtaining clustered rate matrices is variational in the second eigenvalue. This suggests that the second eigenvalue can be used as a variational parameter for identifying optimal clustering boundaries.[39] Furthermore, we also showed in analytical examples[24] that such optimal boundaries are identical with the ones obtained using the local equilibrium definition at long lagtimes.

These results so far all apply for Markovian systems consisting of a finite set of discrete states. In Secs. III C 1 and III C 2, we work in terms of a potential energy surface along a continuous reaction coordinate x. Using this continuous approach, we aim to identify the optimal position, along the reaction coordinate, which defines the boundary between two clusters of states. For this purpose, we will relate the correlation functions of the clustered system to mean first passage times. This will lead to an expression for the slowest relaxation time that can be explicitly maximized to obtain an optimal boundary choice.

We make the assumption that a discretized approximation of the continuous results of Secs. III C 1 and III C 2 can be related to the previous results for the Hummer-Szabo matrix since Markov state models are assumed to be discrete approximations of some true continuous dynamics.

We also make the assumption that the dynamics of our system can be appropriately described by a single-variable Smoluchowski equation. This is known to be a valid assumption for many systems of biological interest. However, it is likely that the MFPT results of Secs. III C 1 and III C 2 can be generalized to multidimensional dynamics.

1. Two state case

In this section, we consider dynamics in a potential energy surface, along the continuous reaction coordinate x and with the potential being bounded within some finite range $[x_{min}, x_{max}]$. For simplicity of the expressions, we will consider $x_{min} = -\infty$ and $x_{max} = \infty$ and assume that the potential energy goes to infinity at some finite boundaries, or, alternatively, the populations vanish outside the finite range. This will ensure that we have a finite Markov chain when discretizing the continuous problem.

Our system is clustered into two states termed regions 1 and 2 and separated by a dividing surface at $x = a$ (such that states 1 and 2 correspond to the ranges of x values less than a and more than a, respectively). In this case, the correlation matrix contains only one independent element. From the fluctuation-dissipation theorem, it can be easily shown that the integral of the normalized correlation function is related to the relaxation time of the system ($\tau_2(a)$, dependent on the boundary position as the single independent parameter)[47,49,51]

$$\tau_2(a) = \int_0^\infty \frac{\tilde{C}_{11}(t)}{\tilde{C}_{11}(0)}dt = \int_0^\infty \frac{\langle \delta\theta_1(0)\delta\theta_1(t)\rangle}{\langle \delta\theta_1(0)^2\rangle}dt, \tag{39}$$

where $\delta\theta_1(x) = \theta_1(x) - \langle\theta_1\rangle$ and $\theta_1(x)$ is the two-state number function

$$\theta_1(x) = \begin{cases} 1 & \text{for} \quad x \le a \\ 0 & \text{for} \quad x > a. \end{cases} \tag{40}$$

Earlier results exploited the properties of the θ_1 function to arrive at Eq. (41) (see Appendix D).[48,50] Here, t_{a1} represents the mean time taken to reach a barrier placed at position a given an initial starting position within region 1 which spans $(-\infty, a]$

$$\tau_2(a) = p_1^{eq} t_{a2} + p_2^{eq} t_{a1}. \tag{41}$$

To obtain the choice of dividing surface which maximizes the value of $\tau_2(a)$, Eq. (41) can be explicitly differentiated with respect to a (see Appendix E). This gives that the maximum value of $\tau_2(a)$ occurs when the condition in Eq. (42) is satisfied. This condition is equivalent to the requirement that the fluxes crossing the boundary in each direction are equal

$$p_1^{eq} t_{a2} = p_2^{eq} t_{a1}. \tag{42}$$

Substituting this result back into Eq. (41) and using the detailed balance condition together with the relation between the relaxation time and the inter-state transition rates, $\tau_2 = 1/(R_{12} + R_{21})$ (which are both automatically satisfied for a two state Markovian system), give the following result for the reduced rate constants:

$$R_{12} = \frac{1}{2t_{a2}} \tag{43}$$

and

$$R_{21} = \frac{1}{2t_{a1}}. \tag{44}$$

This is a remarkable result, related to the stochastic separatrix,[52,53] which shows that at the optimal dividing surface between two clusters the probability to move in either direction is 1/2.

2. Three state symmetric case

Ideally, one would like to extend this type of analysis to the three-state case and beyond. However, as the number of clustered states increases, so does the number of free parameters in the correlation matrix. To limit the number of free parameters, we restrict here the system to be symmetric. This reduces the problem to finding only one boundary a, the other being located at $-a$ because of symmetry (so that our three states, 1, 2, and 3, are defined by $x < -a$, $-a < x < a$, and $x > a$, respectively, assuming a positive). It can then be shown that the second eigenvalue is related to the correlation functions via

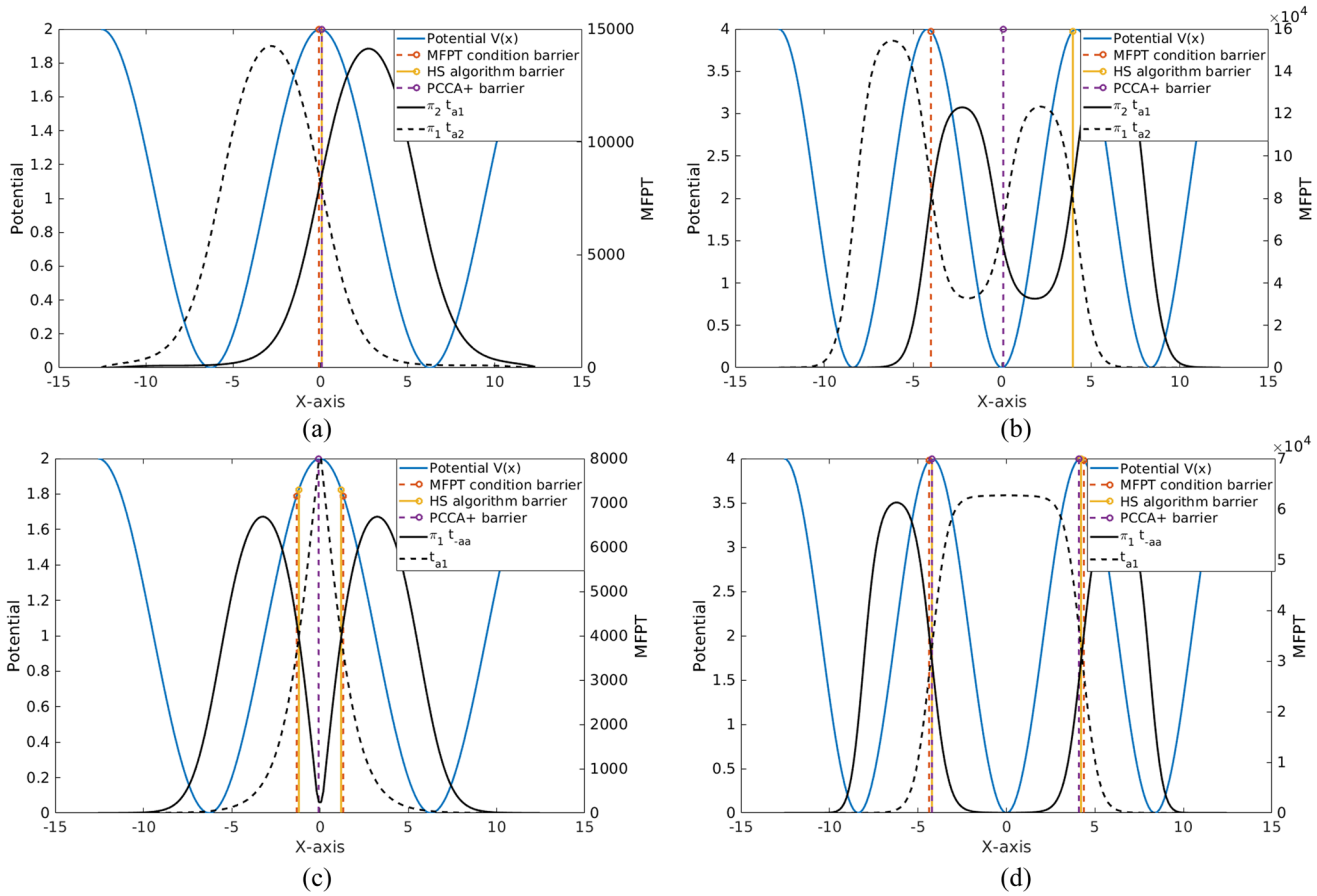

FIG. 1. Clustering of a double [(a) and (c)] and triple [(b) and (d)] well potential (blue line) into two [(a) and (b)] and three [(c) and (d)] states using variational Hummer-Szabo optimization (orange solid stem plot), the MFPTs by Eqs. (42) and (47) (red dashed stem plot), and the PCCA+ method (purple dashed stem plot). The solid and dashed black lines show the MFPT quantities on the left and right side of equations (42) [(a) and (b)] and (47) [(c) and (d)], respectively, which are equal at the derived optimal MFPT boundary. (a) Two state clustering. (b) Two state clustering. (c) Three state clustering. (d) Three state clustering.

$$\tau_2(a) = \frac{1}{p_1^{eq}}\left(2\int_0^\infty \frac{\bar{C}_{11}(t)}{\bar{C}_{11}(0)}dt + \int_0^\infty \frac{\bar{C}_{12}(t)}{\bar{C}_{12}(0)}dt\right). \quad (45)$$

Performing a similar analysis as described earlier, it can be shown that the second eigenvalue is given exactly in terms of MFPTs (see Appendix F for full details)

$$\tau_2(a) = p_1^{eq} t_{-aa} + t_{-a1}. \quad (46)$$

Here, t_{-aa} describes the time to move from a to $-a$ (the positions of the two boundaries defining a three state clustering in a symmetric potential). As described earlier, this expression can be differentiated with respect to the position of the boundary a to find the condition which optimizes the relaxation time (see Appendix F)

$$p_1^{eq} t_{-aa} = t_{-a1}. \quad (47)$$

This condition equates the flux of particles leaving state 1 to the rate with which particles cross from $-a$ to a (through the middle state).

IV. COMPUTATIONAL VERIFICATION OF RESULTS

A. Analytic examples

The equations derived in this report are tested by applying them to some simple analytic test cases, in particular, double and triple well potentials. The rate matrices are constructed by assuming Arrhenius rates for the potential in question

$$k_{ji} = Ae^{-\frac{v(j)-v(i)}{2K_BT}}. \quad (48)$$

The potential is generated by discretizing the x-axis (ranging from -4π to 4π) into 800 data points and calculating $v(x)$ at each x value. We implement two different methods for determining the optimal clustering, the Hummer-Szabo method and the MFPT method, and compare their performance with the broadly used PCCA+ method.[28] The Hummer-Szabo method is implemented by using Eq. (12) from Ref. 39 to obtain a reduced rate matrix and then iterating over each choice of clustering to find the rate matrix with the maximal relaxation time. The MFPT method computes the mean first passage times using the Meyer method[54,55] between states on a Markov chain and finds the optimal clustering as the one that gives MFPT values which satisfy the conditions derived in Sec. III C.

1. Analytic double and triple well potentials

The first examples considered are symmetric potentials, with double and triple wells, as shown in Fig. 1. These potentials are described by Eqs. (49) and (50), respectively (where the values c_0 and c_1 are chosen such that $v(x)$ takes the minimum value 0 in the range -4π to 4π)

$$v(x) = -\sin\left(\frac{x-\pi}{2}\right) + c_0, \quad (49)$$

$$v(x) = \sin\left(\frac{1.5x-\pi}{2}\right) + c_1. \quad (50)$$

In the two state double well clustering, it is intuitive to expect that the top of the barrier is identified as the optimal two state boundary position. Similarly, in the three state triple well clustering, it is expected for the optimal boundary to cluster the state space into three equal states. As shown in Fig. 1, either using the variational Hummer-Szabo method or by applying the derived MFPT equations, the exact same boundaries are found, and moreover, in the double well two-state clustering and triple well three-state clustering, these boundaries are what we would expect to see intuitively. In the two-state clustering of the triple well potential, Eq. (42) is satisfied in three locations but since the derivation was for a condition where the relaxation time is extremized, two of these positions maximize the relaxation time while the other position is a local minimum. In contrast, the PCCA+ method can find the same clusters when it is identifying metastable states [as in Figs. 1(a) and 1(d)]; however, it does not find a transition state when asked to find more or less clusters than the existing stable states [as in Figs. 1(b) and 1(c)]. For example, in Fig. 1(b), the third metastable state gets divided between the other two clusters, while in Fig. 1(c), the PCCA+ algorithm finds two stable clusters and a third cluster of size zero in between.

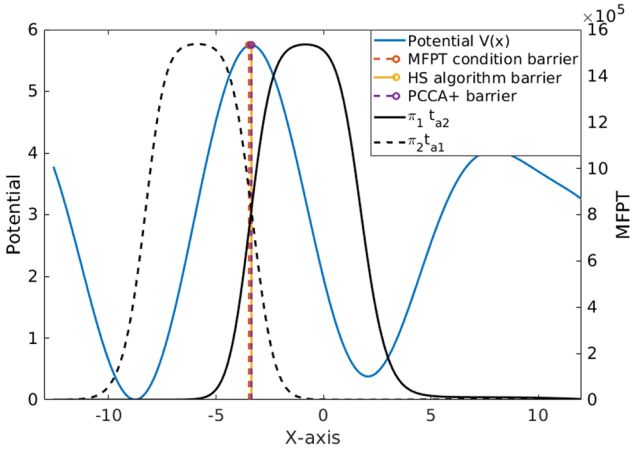

FIG. 2. Two state clustering on an asymmetric double well potential (blue line): The same optimal boundary positions are predicted by the MFPT (red dashed line), Hummer-Szabo (orange line), and PCCA+ (purple line) clustering methods. The optimal boundary in the MFPT method is defined by the position at which the MFPT quantities (black solid and dashed lines) intersect.

2. Asymmetric potential

To test the generality of Eq. (42), we implemented it on an asymmetric potential, shown in Fig. 2 and described as follows:

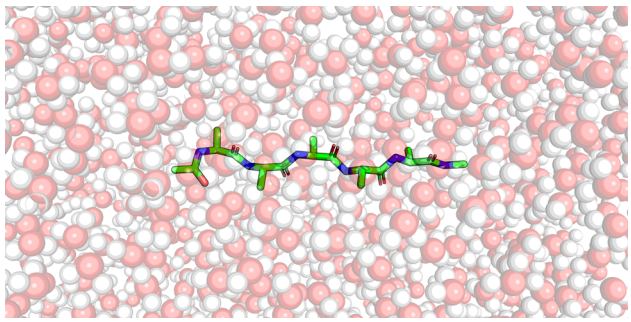

FIG. 3. Illustration of the Ala_5 simulation system.

$$v(x) = \sin\left(\frac{x-\pi}{2}\right) + \sin(0.7(x-\pi)) + c_2. \quad (51)$$

The three state MFPT equation cannot be tested on this potential as the derivation assumes a symmetric potential. By implementing the variational Hummer-Szabo definition and searching through all possible boundary positions, the exact same boundaries are found when Eq. (42) is used, thereby demonstrating that Eq. (42) holds for general potentials.

For comparison, PCCA+ is also implemented and finds the same clusters as the Hummer-Szabo method since we are just identifying stable states.

B. MD pentalanine simulations

The next test of the derived equations is to demonstrate that they hold true when examining MD simulation data. We performed MD simulations of pentalanine in explicit water (Fig. 3), using CHARMM-GUI (graphical user interface) for setting up the system. The ligand was capped with an ACE at the N terminus and an NME group at the C terminus. The ligand was solvated in an explicit water box. The simulations were run using NAMD[56] at a temperature of 300 K and a time step of 2 fs with a Langevin thermostat. A total of 1 microsecond production run was performed. To test the derived equations in this paper, the 10 backbone dihedral angles (Φ, Ψ) of

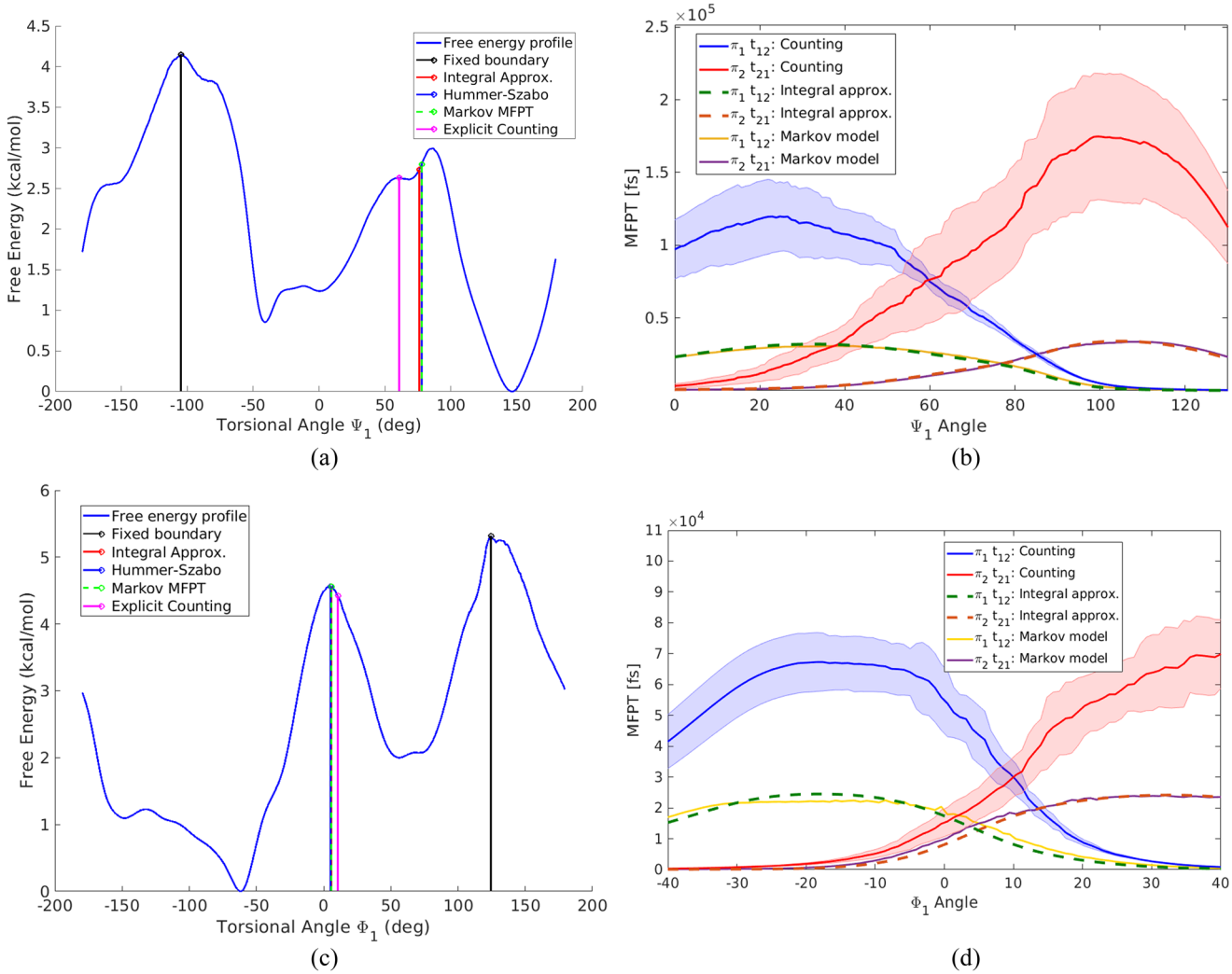

FIG. 4. Two state clustering for Ala_5 dihedral angles Ψ_1 [(a) and (b)] and Φ_1 [(c) and (d)]. The calculated optimal boundaries [(a) and (c)] for the Hummer-Szabo (blue stem plot) and integral approximation (red stem plot) are found to have almost identical values, while the explicit counting method (pink stem plot) is remarkably close to the true value. In (a) and (c), the free energy profiles (blue curve) with optimal barrier positions are shown together with the fixed boundaries (black stem plot corresponds to the free energy maximum). In (b) and (d), the mean first passage times are calculated as a function of the boundary position from transition counts (solid red and blue lines with error bars), from MSMs (yellow and purple solid lines) and using the approximate integrals (green and red dashed lines). The integral approximation is scaled to match the Markov model MFPTs by estimating the diffusion coefficient. Error bars are obtained from 4 equal segments of the MD simulation trajectory.

the peptide are extracted from the simulation data. As an example, here, we used Ψ_1 and Φ_1 to construct Markov models from which the mean first passage times can be extracted (Fig. 4). The corresponding figures for the additional 8 angles (Ψ_{2-5} and Φ_{2-5}) are provided in the supplementary material.

1. Estimating MFPTs from MD simulation data

There are a number of ways to estimate the MFPTs from simulation data. For completeness, we implemented a variety of methods for estimating the MFPTs in Eq. (41) and verified that they produce equivalent estimates for the optimal boundary position as the Hummer-Szabo algorithm based on the slowest relaxation times.

a. MFPT from Markov model. The first option is to construct a maximum likelihood Markov state model from the simulation data.[5] We used the Meyer method[54,55] to calculate MFPTs from the obtained discrete state Markov model, which requires solving a system of simple linear equations of the following form:

$$t_{ji} = \tau + \sum_{j' \neq j} M_{j'i}(\tau) t_{jj'}, \tag{52}$$

where $M_{ji}(\tau)$ is the Markovian transition probability to make a transition from i to j in the time interval τ and t_{ij} is the MFPT from state i to j. This algorithm is very fast and simple to implement; furthermore, it can also be more efficient than the Hummer-Szabo algorithm as it does not require the diagonalization of the Markov matrix.

b. Explicit counting from MD trajectories. For a time series of discrete states $\mathbf{x} = x_1, x_2, \ldots, x_n$ with timestep τ, one can estimate the mean passage time to leave a region and hit a boundary at $x = a$ by explicit counting directly from the MD simulation trajectories.

If we observe the system to hit the boundary at times T_1, T_2, $T_3, \ldots, T_k$, starting, for example, in state 2, then the number of steps spent in state 1 will be given by $N_1 = \frac{T_2 - T_1}{\tau}$, $N_2 = \frac{T_4 - T_3}{\tau}$, and so on, as demonstrated in Fig. 5.

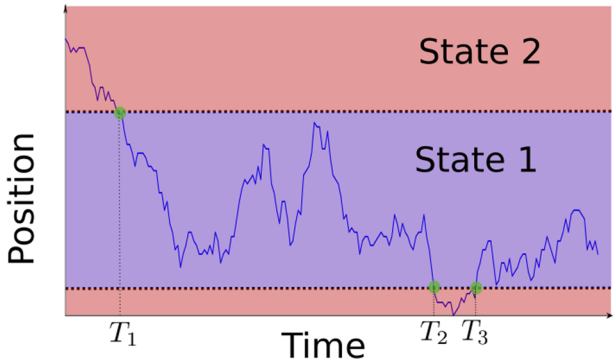

FIG. 5. Illustration of calculating MFPTs by explicit counting on a periodic coordinate. To obtain an estimate for the MFPT between states, we first obtain the times of all boundary crossing events and then use these times as inputs for Eq. (53).

We can maximally make use of the information in our trajectory by considering the MFPT from each microstate to the boundary. For crossing event i, we observe an instance of a trajectory of length N_i to the boundary. This is then immediately followed by an observed trajectory of length $N_i - 1$ to the boundary and so on until we observe a trajectory of length 1 to the boundary. The MFPT from a single crossing event can then be approximated by obtaining the sum of all these observed trajectories for all relevant events (in a trajectory with k total crossing events, there will be $k/2$ crossing events which contribute to the MFPT of interest, i.e., from state 1 to 2). To normalize with respect to the total simulation time, we divide by the total length spent in state 1

$$\frac{\sum_i^{k/2} \sum_{j=1}^{N_i} j}{\sum_i^{k/2} N_i} = \frac{\sum_i^{k/2} (N_i + 1) N_i / 2}{\sum_i^{k/2} N_i}. \tag{53}$$

Here, we also assume that over long simulation times, each microstate is explored with equilibrium probabilities. This algorithm, in principle, only requires identifying the boundary crossing times over the trajectories; therefore, it can be more efficient than the previous approaches. However, as it requires sufficiently well converged "equilibrium" trajectories, its numerical error that also includes non-Markovian effects can be larger.

c. Discrete approximation of integrals assuming a constant diffusion coefficient. As an alternative method, we can express the quantities in Eq. (41) as integrals (as detailed in Appendix E) and estimate them numerically. Since we do not know the value of the diffusion constant D, the MFPTs estimated will not be of the correct magnitude. They will however be proportional to the true value and regardless of the magnitude of D, the crossing point defining the optimal boundary can be obtained. By comparing the integrals to the MFPTs from our counting method, we can estimate the diffusion constant D by scaling the integration approximation of MFPTs to match the observed values, assuming that D is constant along the free energy profile. From a computational efficiency perspective, the discrete approximation method can be much more efficient than Hummer-Szabo method, if the equilibrium populations can be estimated from the trajectories, otherwise it is of similar magnitude, as it requires the first eigenvector of the maximum likelihood Markov matrix.

The applications to the dihedral angles of Ala5 require taking into account periodic reaction coordinates. By fixing one boundary at the point of maximum free energy, the problem becomes a single barrier optimization problem. We implemented both the explicit counting procedure and the integral approximation method to estimate the MFPTs in Eq. (41), as well as the Hummer-Szabo method. We find that they result in almost identical boundary placements, as shown in Fig. 4. In particular, the numerical error of the explicit counting is smaller when the Φ_1 angle is used [Fig. 4(c)], which has a larger free energy barrier than Ψ_1 [Fig. 4(a)]; therefore, the resulting two state system is more Markovian. Our results also show that the constant diffusion coefficient assumption is an excellent approximation in this system, as the numerical integral approximation in Figs. 4(b) and 4(d) matches almost perfectly the MFPTs obtained

from the Markov model, which does not rely on this assumption. The fitted diffusion coefficients are $D \approx 1.82$ deg^2/fs for Ψ_1 and $D \approx 3.85$ deg^2/fs for Φ_1.

V. CONCLUSIONS AND OUTLOOK

Here we reviewed the requirements for clustering high-dimensional Markovian dynamics and offer novel definitions for the coarse-grained Markovian dynamics. We propose a new general definition that satisfies a variational principle, and the slowest relaxation time of the reduced system is never slower than that of the original full-dimensional system. Special cases of this definition correspond to the Hummer-Szabo and the local equilibrium methods. These results verify the empirical observation made in previous studies that the slowest relaxation time of the clustered model can be used to variationally identify metastable and transition states.[24]

In addition, the Hummer-Szabo method, which enforces the time integrated correlation functions of the full and reduced systems to be exact, is examined in further detail. We have previously demonstrated[24] that the Hummer Szabo (HS) scheme leads to the same optimal boundaries as the local equilibrium scheme with long lagtimes; therefore, our results apply to optimal coarse graining more generally. We describe the time integrated correlation functions in terms of mean first passage times along a 1-D potential. We derived that the variationally optimal two-state coarse graining leads to boundaries that have equal fluxes crossing through them. Remarkably, these optimal boundaries are also identified as the stochastic separatrix, a dividing surface with equal probability to move in either direction.

Our results are also tested on analytic and MD simulation examples. Using discretized rate matrices of analytic free energy profiles, we demonstrate that variational two-state clustering using the Hummer-Szabo method produces identical boundary positions as the stochastic separatrix. Furthermore, the three-state coarse graining procedure also reproduces the boundary positions exactly according to the derived expressions, currently restricted to symmetric potentials.

The derived equations were tested on free energy profiles obtained from MD simulations of pentalanine. We demonstrated that the derived equations provide equivalent cluster boundaries to the variational Hummer-Szabo method. Very similar optimal boundary positions are also found by approximating the mean first passage times explicitly, counting transitions from the trajectory data.

The MFPT condition approach to obtaining the transition state will typically be similarly computationally efficient as the Hummer-Szabo method. Explicit counting can highlight numerical differences from the MSM-based MFPTs and could signal the presence of non-Markovian behavior.

While we showed here that the second eigenvalue is variational and that using it as an optimization protocol leads to physically intuitive results, it is possible to imagine that there may be other quantities that could be suitable parameters for defining "optimal" coarse graining. Additionally, a physical interpretation of clustering into more than two states in a general potential or in higher dimensions is still currently missing.

In summary, bringing together definitions and known relationships across mean first passage times, correlation functions and continuous reactive dynamics allowed us to derive simple flux relations, which provide intuitive interpretations and justification to obtain variationally optimal coarse-grained clustering boundaries.

SUPPLEMENTARY MATERIAL

See supplementary material for free energy figures of all ala5 Ramachandran angles.

ACKNOWLEDGMENTS

We gratefully thank Attila Szabo (NIDDK, NIH), who supported this work through a number of discussions and suggestions. We also thank Ágnes Szabados and Péter Surján (Laboratory of Theoretical Chemistry, ELTE Eötvös Loránd University) for their collaboration on this project. E.R. acknowledges funding from EPSRC (EP/R013012/1, EP/L027151/1, and EP/N020669/1) and the ERC (Project No. 757850 BioNet). A.K. was supported by the EPSRC Centre for Doctoral Training in Cross-Disciplinary Approaches to Non-Equilibrium Systems (CANES, EP/L015854/1). Zs.É.M. was supported by the ÚNKP-18-3 New National Excellence Program of the Ministry of Human Capacities. We are grateful to the UK Materials and Molecular Modelling Hub for computational resources, which is partially funded by EPSRC (EP/P020194/1).

APPENDIX A: DETAILED BALANCE FOR GENERAL LAPLACE VARIABLE *s*

We demonstrate that the Laplace transformed rate matrix [Eq. (23)] of the coarse-grained system resulting from projection $\mathcal{P}$ satisfies detailed balance for arbitrary values of s, as soon as the rate matrix of the original system does. Multiplying Eq. (23) times $\mathbf{D}_N$ from right, we have

$$\hat{\mathbf{R}}(s)\mathbf{D}_N = s\mathbf{A}^T\mathbf{K}(s\mathbf{I}_n - \mathbf{K} + \mathbf{D}_n\mathbf{A}\mathbf{D}_N^{-1}\mathbf{A}^T\mathbf{K})^{-1}\mathbf{D}_n\mathbf{A}. \tag{A1}$$

The above equation can be rewritten in terms of the symmetric rate matrix

$$\hat{\mathbf{R}}(s)\mathbf{D}_N = s\mathbf{A}^T\mathbf{D}_n^{1/2}\mathbf{K}_{sym}\mathbf{D}_n^{-1/2}\big(s\mathbf{D}_n^{1/2}\mathbf{D}_n^{-1/2} - \mathbf{D}_n^{1/2}\mathbf{K}_{sym}\mathbf{D}_n^{-1/2} + \mathbf{D}_n\mathbf{A}\mathbf{D}_N^{-1}\mathbf{A}^T\mathbf{D}_n^{1/2}\mathbf{K}_{sym}\mathbf{D}_n^{-1/2}\big)^{-1}\mathbf{D}_n\mathbf{A}. \tag{A2}$$

Since every term within the inverse is of the form $\mathbf{D}_n^{1/2}\mathbf{X}\mathbf{D}_n^{-1/2}$, the $\mathbf{D}$ terms can be taken outside of the inverse, resulting in some cancellation

$$\hat{\mathbf{R}}(s)\mathbf{D}_N = s\mathbf{A}^T\mathbf{D}_n^{1/2}\mathbf{K}_{sym}\big(s\mathbf{I}_n - \mathbf{K}_{sym} + \mathbf{D}_n^{-1/2}\mathbf{A}\mathbf{D}_N^{-1}\mathbf{A}^T\mathbf{D}_n^{1/2}\mathbf{K}_{sym}\big)^{-1}\mathbf{D}_n^{1/2}\mathbf{A}. \tag{A3}$$

It is sufficient to just examine the middle section since the $\mathbf{A}$ and $\mathbf{D}$ terms appear on both sides of the expression

$$\mathbf{K}_{sym}\big(s\mathbf{I}_n + \big(-\mathbf{I}_n + \mathbf{D}_n^{-1/2}\mathbf{A}\mathbf{D}_N^{-1}\mathbf{A}^T\mathbf{D}_n^{1/2}\big)\mathbf{K}_{sym}\big)^{-1}. \tag{A4}$$

This inverse can then be calculated using the Woodbury inversion formula used in the main text

$$(\mathbf{M} + \mathbf{U}\mathbf{V})^{-1} = \mathbf{M}^{-1} - \mathbf{M}^{-1}\mathbf{U}(\mathbf{I}_n + \mathbf{V}\mathbf{M}^{-1}\mathbf{U})\mathbf{V}\mathbf{M}^{-1}. \tag{A5}$$

This formula is implemented with $\mathbf{M} = s\mathbf{I}_n$, $\mathbf{U} = \left(-\mathbf{I}_n + \mathbf{D}_n^{-1/2}\mathbf{A}\mathbf{D}_N^{-1}\mathbf{A}^T\mathbf{D}_n^{1/2}\right)$, and $\mathbf{V} = \mathbf{K}_{sym}$ to obtain the following equation, where $\mathbf{X} = \mathbf{D}_n^{1/2}\mathbf{A}\mathbf{D}_N^{-1}\mathbf{A}^T\mathbf{D}_N^{1/2}$:

$$\frac{1}{s}\mathbf{K}_{sym} - \frac{1}{s}\mathbf{K}_{sym}(-\mathbf{I}_n + \mathbf{X}) - \frac{1}{s^3}\mathbf{K}_{sym}(-\mathbf{I}_n + \mathbf{X})\mathbf{K}_{sym}(-\mathbf{I}_n + \mathbf{X})\mathbf{K}_{sym}. \tag{A6}$$

Our expression has many symmetric quantities—$\mathbf{K}_{sym}$ is symmetric and $\mathbf{X}$ (and hence $(-\mathbf{I}_n + \mathbf{X})$) is symmetric—therefore, the first and third terms are clearly symmetric. It remains only to examine whether the second term $\mathbf{K}_{sym}(-\mathbf{I}_n + \mathbf{X})$ is symmetric. To see that this quantity is symmetric, one can consider instead $\mathbf{A}^T\mathbf{D}_n^{1/2}\mathbf{K}_{sym}\mathbf{X}\mathbf{D}_n^{1/2}\mathbf{A}$ [since this is how it will appear when it is resubstituted into Eq. (A3)]

$$\begin{aligned}\mathbf{A}^T\mathbf{D}_n^{1/2}\mathbf{K}_{sym}\mathbf{X}\mathbf{D}_n^{1/2}\mathbf{A} &= \mathbf{A}^T\mathbf{D}_n^{1/2}\mathbf{K}_{sym}\mathbf{D}_n^{1/2}\mathbf{A}\mathbf{D}_N^{-1}\mathbf{A}^T\mathbf{D}_n\mathbf{A} \\ &= \mathbf{A}^T\mathbf{D}_n^{1/2}\mathbf{K}_{sym}\mathbf{D}_n^{1/2}\mathbf{A}.\end{aligned} \tag{A7}$$

Since this term is also symmetric, it can be seen that the Laplace transformed rate matrix will satisfy detailed balance as desired.

APPENDIX B: VARIATIONAL PRINCIPLE FOR GENERAL TIME INTEGRAL

A possible choice for the reduced matrix $\mathbf{R}$ can be obtained if it is required that for some given times τ_1 and τ_2, the relation in Eq. (B1) holds

$$\begin{aligned}\int_{\tau_1}^{\tau_2}\sum_{i\in I, j\in J}\overline{C}_{ij}(t)\mathrm{d}t &= \int_{\tau_1}^{\tau_2}\overline{C}_{IJ}^{CG}(t)\mathrm{d}t, \\ \int_{\tau_1}^{\tau_2}\sum_{i\in I, j\in J}(e^{\mathbf{K}t})_{ij}p_j\mathrm{d}t &= \int_{\tau_1}^{\tau_2}(e^{\mathbf{R}t})_{IJ}P_J\mathrm{d}t.\end{aligned} \tag{B1}$$

This is equivalent to the following matrix equation (integration meant element-wise):

$$\begin{aligned}&\int_{\tau_1}^{\tau_2}\mathbf{A}^{\mathrm{T}}(e^{\mathbf{K}t}\mathbf{D}_n - \mathbf{p}\mathbf{p}^{\mathrm{T}})\mathbf{A}\mathrm{d}t \\ &= \int_{\tau_1}^{\tau_2}(e^{\mathbf{R}t}\mathbf{D}_N - \mathbf{P}\mathbf{P}^{\mathrm{T}})\mathrm{d}t \\ &= \int_{\tau_1}^{\tau_2}\mathbf{D}_N^{-1/2}\mathbf{A}^{\mathrm{T}}(e^{\mathbf{K}t}\mathbf{D}_n - \mathbf{p}\mathbf{p}^{\mathrm{T}})\mathbf{A}\mathbf{D}_N^{-1/2}\mathrm{d}t \\ &= \int_{\tau_1}^{\tau_2}(\mathbf{D}_N^{-1/2}e^{\mathbf{R}t}\mathbf{D}_N^{1/2} - \mathbf{D}_N^{-1/2}\mathbf{P}\mathbf{P}^{\mathrm{T}}\mathbf{D}_N^{-1/2})\mathrm{d}t.\end{aligned} \tag{B2}$$

As $\mathbf{K} = \mathbf{D}_n^{1/2}\mathbf{K}_{\mathrm{sym}}\mathbf{D}_n^{-1/2}$, the exponential of $\mathbf{K}t$ is $e^{\mathbf{K}t} = \mathbf{D}_n^{1/2}e^{\mathbf{K}_{\mathrm{sym}}t}\mathbf{D}_n^{-1/2}$, where $e^{\mathbf{K}_{\mathrm{sym}}t}$ is also a symmetric matrix, with eigenvalues $1 = e^{\lambda_1 t} > e^{\lambda_2 t} \geq \ldots \geq e^{\lambda_n t} > 0$ and eigenvectors of the form $\mathbf{u}_{n'} = D_n^{-1/2}\mathbf{\Psi}_{n'}^{\mathrm{R}} = D_n^{1/2}\mathbf{\Psi}_{n'}^{\mathrm{L}}$ (independent of t), and in particular, $\mathbf{u}_1 = \mathbf{D}_n^{-1/2}\mathbf{p}$. Therefore, $e^{\mathbf{K}_{\mathrm{sym}}t}$ has the spectral form $\sum_{n'=1}^{n}e^{\lambda_{n'}t}\mathbf{u}_{n'}\mathbf{u}_{n'}^{\mathrm{T}}$. So the integrand on the lhs of Eq. (B2) is a symmetric matrix. Its integral can be evaluated as

$$\begin{aligned}&\int_{\tau_1}^{\tau_2}\mathbf{D}_N^{-1/2}\mathbf{A}^{\mathrm{T}}\mathbf{D}_n^{1/2}(e^{\mathbf{K}_{\mathrm{symm}}t} - \mathbf{u}_1\mathbf{u}_1^{\mathrm{T}})\mathbf{D}_n^{1/2}\mathbf{A}\mathbf{D}_N^{-1/2}\mathrm{d}t \\ &= \int_{\tau_1}^{\tau_2}\mathbf{D}_N^{-1/2}\mathbf{A}^{\mathrm{T}}\mathbf{D}_n^{1/2}\sum_{n'=2}^{n}e^{\lambda_{n'}t}\mathbf{u}_{n'}\mathbf{u}_{n'}^{\mathrm{T}}\mathbf{D}_n^{1/2}\mathbf{A}\mathbf{D}_N^{-1/2}\mathrm{d}t \\ &= \mathbf{D}_N^{-1/2}\mathbf{A}^{\mathrm{T}}\mathbf{D}_n^{1/2}\sum_{n'=2}^{n}\int_{\tau_1}^{\tau_2}e^{\lambda_{n'}t}\mathrm{d}t\,\mathbf{u}_{n'}\mathbf{u}_{n'}^{\mathrm{T}}\mathbf{D}_n^{1/2}\mathbf{A}\mathbf{D}_N^{-1/2} \\ &= \mathbf{D}_N^{-1/2}\mathbf{A}^{\mathrm{T}}\mathbf{D}_n^{1/2}\left(\sum_{n'=2}^{n}\frac{e^{\lambda_{n'}\tau_2} - e^{\lambda_{n'}\tau_1}}{\lambda_{n'}}\mathbf{u}_{n'}\mathbf{u}_{n'}^{\mathrm{T}}\right)\mathbf{D}_n^{1/2}\mathbf{A}\mathbf{D}_N^{-1/2}.\end{aligned} \tag{B3}$$

The matrix $\mathbf{K}_{\mathrm{int}}(\tau_1\tau_2) = \left(\sum_{n'=2}^{n}\frac{e^{\lambda_{n'}\tau_2} - e^{\lambda_{n'}\tau_1}}{\lambda_{n'}}\mathbf{u}_{n'}\mathbf{u}_{n'}^{\mathrm{T}}\right)$ is already in spectral form; its eigenvalues are 0 and $\frac{e^{\lambda_{n'}\tau_2} - e^{\lambda_{n'}\tau_1}}{\lambda_{n'}}$ $(2 \leq n' \leq n)$, so its largest eigenvalue is actually $\frac{e^{\lambda_2\tau_2} - e^{\lambda_2\tau_1}}{\lambda_2}$. For brevity, we will define the vector $\boldsymbol{\tau} = (\tau_1, \tau_2)$. Making use of the function (defined for $\lambda < 0$ to avoid any divergence issues)

$$f_{\boldsymbol{\tau}}(\lambda) = \int_{\tau_1}^{\tau_2}e^{\lambda t}\mathrm{d}t = \frac{e^{\lambda\tau_2} - e^{\lambda\tau_1}}{\lambda}, \tag{B4}$$

which is strictly increasing (for $\tau_2 > \tau_1 > 0$), makes it apparent that $\frac{e^{\lambda_2\tau_2} - e^{\lambda_2\tau_1}}{\lambda_2} \geq \frac{e^{\lambda_3\tau_2} - e^{\lambda_3\tau_1}}{\lambda_3} \geq \cdots \geq \frac{e^{\lambda_n\tau_2} - e^{\lambda_n\tau_1}}{\lambda_n} > 0$ provided that the ordering of the $\lambda_{n'}$ eigenvalues was decreasing.

The matrix in Eq. (B3) is a symmetric matrix, denoted by $\mathbf{B}(\boldsymbol{\tau})$ with eigenvalues $\alpha_{N'}(\boldsymbol{\tau})$ and orthonormal eigenvectors $\mathbf{v}_{N'}(\boldsymbol{\tau})$ $(1 \leq N' \leq N)$. Let $\tilde{\mathbf{u}}_{N'}(\boldsymbol{\tau}) = \mathbf{D}_n^{1/2}\mathbf{A}\mathbf{D}_N^{-1/2}\mathbf{v}_{N'}(\boldsymbol{\tau})$ $(1 \leq N' \leq N)$. These vectors are normalized

$$\begin{aligned}\tilde{\mathbf{u}}_{N'}(\boldsymbol{\tau})^{\mathrm{T}}\tilde{\mathbf{u}}_{N'}(\boldsymbol{\tau}) &= \mathbf{v}_{N'}(\boldsymbol{\tau})^{\mathrm{T}}\mathbf{D}_N^{-1/2}\mathbf{A}^{\mathrm{T}}\mathbf{D}_n^{1/2}\mathbf{D}_n^{1/2}\mathbf{A}\mathbf{D}_N^{-1/2}\mathbf{v}_{N'}(\boldsymbol{\tau}) \\ &= \mathbf{v}_{N'}(\boldsymbol{\tau})^{\mathrm{T}}\mathbf{D}_N^{-1/2}\mathbf{A}^{\mathrm{T}}\mathbf{D}_n\mathbf{A}\mathbf{D}_N^{-1/2}\mathbf{v}_{N'}(\boldsymbol{\tau}) \\ &= \mathbf{v}_{N'}(\boldsymbol{\tau})^{\mathrm{T}}\mathbf{D}_N^{-1/2}\mathbf{D}_N\mathbf{D}_N^{-1/2}\mathbf{v}_{N'}(\boldsymbol{\tau}) \\ &= \mathbf{v}_{N'}(\boldsymbol{\tau})^{\mathrm{T}}\mathbf{v}_{N'}(\boldsymbol{\tau}) = 1.\end{aligned} \tag{B5}$$

This means that $\tilde{\mathbf{u}}_{N'}(\boldsymbol{\tau}) = \sum_{n'=1}^{n}c_{N',n'}(\boldsymbol{\tau})\mathbf{u}_{n'}$, where $\sum_{n'=1}^{n}c_{N,n'}^2(\boldsymbol{\tau}) = 1$, and $c_{N',n'}(\boldsymbol{\tau}) = \mathbf{u}_{n'}^{\mathrm{T}}\tilde{\mathbf{u}}_{N'}(\boldsymbol{\tau})$, so

$$\begin{aligned}\alpha_{N'}(\boldsymbol{\tau}) &= \mathbf{v}_{N'}(\boldsymbol{\tau})^{\mathrm{T}}\mathbf{B}(\boldsymbol{\tau})\mathbf{v}_{N'}(\boldsymbol{\tau}) \\ &= \mathbf{v}_{N'}(\boldsymbol{\tau})^{\mathrm{T}}\mathbf{D}_N^{-1/2}\mathbf{A}^{\mathrm{T}}\mathbf{D}_n^{1/2} \\ &\quad\times\left(\sum_{n'=2}^{n}\frac{e^{\lambda_{n'}\tau_2} - e^{\lambda_{n'}\tau_1}}{\lambda_{n'}}\mathbf{u}_{n'}\mathbf{u}_{n'}^{\mathrm{T}}\right)\mathbf{D}_n^{1/2}\mathbf{A}\mathbf{D}_N^{-1/2}\mathbf{v}_{N'}(\boldsymbol{\tau}) \\ &= \sum_{n'=2}^{n}\frac{e^{\lambda_{n'}\tau_2} - e^{\lambda_{n'}\tau_1}}{\lambda_{n'}}\tilde{\mathbf{u}}_{N'}(\boldsymbol{\tau})^{\mathrm{T}}\mathbf{u}_{n'}\mathbf{u}_{n'}^{\mathrm{T}}\tilde{\mathbf{u}}_{N'}(\boldsymbol{\tau}) \\ &= \sum_{n'=2}^{n}c_{N',n'}^2(\boldsymbol{\tau})\frac{e^{\lambda_{n'}\tau_2} - e^{\lambda\tau_1}}{\lambda_{n'}} \\ &\leq \frac{e^{\lambda_2\tau_2} - e^{\lambda_2\tau_1}}{\lambda_2}\sum_{n'=1}^{n}c_{N',n'}^2(\tau) = \frac{e^{\lambda_2\tau_2} - e^{\lambda_2\tau_1}}{\lambda_2}.\end{aligned} \tag{B6}$$

The last inequality holds because it has been shown that for $n' > 2$ we have $\frac{e^{\lambda_{n'}\tau_2} - e^{\lambda_{n'}\tau_1}}{\lambda_{n'}} \leq \frac{e^{\lambda_2\tau_2} - e^{\lambda_2\tau_1}}{\lambda_2}$. From Eq. (B6), it is also apparent that $0 \leq \alpha_{N'}(\tau)$. The first eigenvector of $\mathbf{B}(\boldsymbol{\tau})$ is $\mathbf{v}_1(\boldsymbol{\tau}) = \mathbf{D}_N^{-1/2}\mathbf{P}$ belonging

to eigenvalue $\alpha_1(\tau) = 0$. This is evident from $\mathbf{A}^T\mathbf{D}_n\mathbf{A} = \mathbf{D}_N$ and $\mathbf{A}^T\mathbf{D}_n^{1/2}\mathbf{u}_1 = \mathbf{A}^T\mathbf{p} = \mathbf{P}$

$$\begin{aligned}\mathbf{B}(\boldsymbol{\tau})\mathbf{D}_N^{-1/2}\mathbf{P} &= \mathbf{D}_N^{-1/2}\mathbf{A}^{\mathrm{T}}\mathbf{D}_n^{1/2} \\ &\quad\times\left(\sum_{n'=2}^{n}\frac{e^{\lambda_{n'}\tau_2}-e^{\lambda_{n'}\tau_1}}{\lambda_{n'}}\mathbf{u}_{n'}\mathbf{u}_{n'}^{\mathrm{T}}\right)\mathbf{D}_n^{1/2}\mathbf{A}\mathbf{D}_N^{-1/2}\mathbf{D}_N^{-1/2}\mathbf{P} \\ &= \mathbf{D}_N^{-1/2}\mathbf{A}^{\mathrm{T}}\mathbf{D}_n^{1/2}\left(\sum_{n'=2}^{n}\frac{e^{\lambda_{n'}\tau_2}-e^{\lambda_{n'}\tau_1}}{\lambda_{n'}}\mathbf{u}_{n'}\mathbf{u}_{n'}^{\mathrm{T}}\right)\mathbf{u}_1 \\ &= 0. \end{aligned} \tag{B7}$$

Therefore, since $\tilde{\mathbf{u}}_2(\boldsymbol{\tau})$ is normalized, the product $\tilde{\mathbf{u}}_2(\boldsymbol{\tau})^{\mathrm{T}}\mathbf{K}_{\mathrm{int}}(\boldsymbol{\tau})\tilde{\mathbf{u}}_2(\boldsymbol{\tau})$ is going to be a lower bound for the largest eigenvalue of $\mathbf{B}(\boldsymbol{\tau})$, which is $\frac{e^{\lambda_2\tau_2}-e^{\lambda_2\tau_1}}{\lambda_2}$

$$\begin{aligned}\alpha_2(\boldsymbol{\tau}) &= \mathbf{v}_2(\boldsymbol{\tau})^{\mathrm{T}}\mathbf{B}(\boldsymbol{\tau})\mathbf{v}_2(\boldsymbol{\tau}) \\ &= \tilde{\mathbf{u}}_2(\boldsymbol{\tau})^{\mathrm{T}}\mathbf{K}_{\mathrm{int}}(\boldsymbol{\tau})\tilde{\mathbf{u}}_2(\boldsymbol{\tau}) \le \frac{e^{\lambda_2\tau_2}-e^{\lambda_2\tau_1}}{\lambda_2}. \end{aligned} \tag{B8}$$

Using the result proved in Appendix A $\mathbf{R}\mathbf{D}_N = \mathbf{D}_N\mathbf{R}^{\mathrm{T}}$, it follows that $\mathbf{R}_{\mathrm{symm}} = \mathbf{D}_N^{-1/2}\mathbf{R}\mathbf{D}_N^{1/2}$ is a symmetric matrix, with $\boldsymbol{\Phi}_1 = \mathbf{D}_N^{-1/2}\mathbf{P}$ as one of its eigenvectors, corresponding to eigenvalue $\mu_1 = 0$, and with other eigenvalues $0 > \mu_2 \ge \cdots \ge \mu_N$ and corresponding eigenvectors $\boldsymbol{\Phi}_{N'}$ $(2 \le N' \le N)$. This means that the matrix on the rhs of Eq. (B2) is

$$\begin{aligned}\int_{\tau_1}^{\tau_2}(e^{\mathbf{R}_{\mathrm{sym}}t}-\mathbf{D}_N^{-1/2}\mathbf{P}\mathbf{P}^{\mathrm{T}}\mathbf{D}_N^{-1/2})\mathrm{d}t &= \sum_{N'=2}^{N}\int_{\tau_1}^{\tau_2}e^{\mu_{N'}t}\mathrm{d}t\boldsymbol{\Phi}_{N'}\boldsymbol{\Phi}_{N'}^{\mathrm{T}} \\ &= \sum_{N'=2}^{N}f_{\boldsymbol{\tau}}(\mu_{N'})\boldsymbol{\Phi}_{N'}\boldsymbol{\Phi}_{N'}^{\mathrm{T}}. \end{aligned} \tag{B9}$$

But the eigenvalues of the above matrix are already known. They are (besides 0) $\alpha_2(\tau) \ge \cdots \ge \alpha_N(\tau)$. From the monotone increasing property of f_τ, it follows that if $0 > \mu_2 \ge \mu_3 \ge \cdots \ge \mu_N$, then $f_\tau(\mu_2) \ge f_\tau(\mu_3) \ge \cdots \ge f_\tau(\mu_N)$. This way $\alpha_{N'}(\tau) = f_\tau(\mu_{N'})$ for all $N' \ge 2$. Therefore, Eq. (B8) can be written as

$$f_\tau(\mu_2) = \alpha_2(\tau) \le \frac{e^{\lambda_2\tau_2}-e^{\lambda_2\tau_1}}{\lambda_2} = f_\tau(\lambda_2). \tag{B10}$$

Relying once more on the monotonicity of f_τ, it can be concluded that

$$\begin{matrix} f_\tau(\mu_2) \le f_\tau(\lambda_2), \\ \mu_2 \le \lambda_2 \end{matrix}. \tag{B11}$$

APPENDIX C: VARIATIONAL PRINCIPLE OF LOCAL EQUILIBRIUM CONDITION FOR $\tau = 0$

In this section, the variational principle is demonstrated for the local equilibrium condition. The local equilibrium condition corresponds to enforcing that the number of transitions occurring at equilibrium is exact at short times. In the case where $t \ll 1$, then the following simple condition is true:

$$R_{IJ}P_J = \sum_{i\in I}\sum_{j\in J}K_{ij}p_j. \tag{C1}$$

Analogous to the proof for Hummer-Szabo, both sides of this equation can be spectral decomposition

$$\sum_{n'=2}^{N}\mu_{n'}\Phi_{n'}^R(I)\Phi_{n'}^R(J) = \sum_{i\in I}\sum_{j\in J}\sum_{n'=2}^{n}\lambda_{n'}\psi_{n'}^R(i)\psi_{n'}^R(j). \tag{C2}$$

Multiplying both sides by $\Psi_2^L(I)\Psi_2^L(J)$ and summing over all macrostates I and J, the second eigenvalue can be isolated

$$\mu_2 = \sum_{I,J}\sum_{i\in I}\sum_{j\in J}\sum_{n'=2}^{n}\lambda_{n'}\psi_{n'}^R(i)\psi_{n'}^R(j)\Phi_2^L(I)\Phi_2^L(J). \tag{C3}$$

Exactly as before, it follows that $\mu_2 < \lambda_2$ and so (since the eigenvalues are both negative) it follows that $\frac{-1}{\mu_2} < \frac{-1}{\lambda_2}$. Hence, the local equilibrium condition satisfies the variational principle for its second eigenvalue

$$\tau_2^R \le \tau_2^K. \tag{C4}$$

APPENDIX D: DERIVATION OF EQ. (41)

By considering the case of diffusion in some potential $v(x)$ with allowed motion between a and b, the location at which a barrier will maximise the relaxation time can be searched for. Perico and Szabo[49] shows that (where $\beta = \frac{1}{K_B T}$)

$$\int_0^\infty\langle\delta\theta_1(0)\delta\theta_1(t)\rangle = \int_{-\infty}^{\infty}\frac{dx}{De^{-\beta v(x)}}\frac{\left[\int_x^\infty\delta\theta_1(y)e^{-\beta v(y)}dy\right]^2}{\int_{-\infty}^{\infty}e^{-\beta v(x)}dx}. \tag{D1}$$

One can define the probability to occupy a given state within region one by $p_1(x) = \frac{e^{-\beta V(x)}}{\int_{-\infty}^{a}e^{-\beta V(x)}dx}$, and similarly for region 2. Splitting the integral into two segments, one running from $-\infty$ to a (region 1) and the other from a to ∞ (region 2) and exploiting the properties of the number function, it can be shown that

$$\begin{aligned}&\int_0^\infty\langle\delta\theta_1(0)\delta\theta_1(t)\rangle dt \\ &= (1-\langle\theta_1\rangle)^2\frac{\int_{-\infty}^{a}e^{-\beta v(x)}dx}{\int_{-\infty}^{\infty}e^{-\beta v(x)}dx}\int_{-\infty}^{a}\frac{dx}{Dp_1(x)}\left[\int_{-\infty}^{x}p_1(y)dy\right]^2 \\ &\quad+\langle\theta_1\rangle^2\frac{\int_{a}^{\infty}e^{-\beta v(x)}dx}{\int_{-\infty}^{\infty}e^{-\beta v(x)}dx}\int_{a}^{\infty}\frac{dx}{Dp_2(x)}\left[\int_{x}^{\infty}p_2(y)dy\right]^2. \end{aligned} \tag{D2}$$

From Eq. (9) one has $\langle\delta\theta_1(0)^2\rangle = p_1^{eq}(1-p_1^{eq})$

$$\langle\delta\theta_1(0)^2\rangle = \frac{\int_{-\infty}^{a}e^{-\beta v(x)}\int_{a}^{\infty}e^{-\beta v(x)}}{(\int_{-\infty}^{\infty}e^{-\beta v(x)})^2}. \tag{D3}$$

Combining Eqs. (D3) and (D2) with Eq. (39), it can be found that

$$\begin{aligned}\tau_2(a) &= p_2^{eq}\int_{-\infty}^{a}\frac{dx}{Dp_1(x)}\left[\int_{-\infty}^{x}p_1(y)dy\right]^2 \\ &\quad+p_1^{eq}\int_{a}^{\infty}\frac{dx}{Dp_2(x)}\left[\int_{x}^{\infty}p_2(y)dy\right]^2. \end{aligned} \tag{D4}$$

Recognizing that the mean first passage time to the barrier from the positive side is given by

$$t_{a2} = \int_a^\infty \frac{dx}{Dp_2(x)}\left[\int_x^\infty p_2(y)dy\right], \tag{D5}$$

and similarly for the other side of the barrier, Eq. (D4) can be written in the compact form

$$\tau_2(a) = p_2^{eq} t_{a1} + p_1^{eq} t_{a2}. \tag{D6}$$

APPENDIX E: OPTIMAL TWO STATE BOUNDARY

The optimal barrier will be such that the τ_2 is maximized with respect to the barrier position a

$$\frac{d\tau_2}{da} = 0. \tag{E1}$$

This requires the derivative of each of the four components of Eq. (D6). The derivatives of the p terms are straightforward

$$\frac{dp_2^{eq}}{da} = \frac{-e^{-\beta v(a)}}{\int_{-\infty}^\infty e^{-\beta v(x)}dx} = -p(a), \tag{E2}$$

$$\frac{dp_1^{eq}}{da} = \frac{e^{-\beta v(a)}}{\int_{-\infty}^\infty e^{-\beta v(x)}dx} = p(a). \tag{E3}$$

The more difficult term to differentiate is the mean first passage time. This requires use of the Leibniz integral rule

$$\frac{d}{dx}\left(\int_{a(x)}^{b(x)} f(x,t)\,\mathrm{d}t\right) = f(x,b(x))\cdot b'(x) - f(x,a(x))\cdot a'(x) + \int_{a(x)}^{b(x)} \frac{\partial}{\partial x} f(x,t). \tag{E4}$$

Applying this gives the following result for the mean first passage terms:

$$\frac{dt_{a2}}{da} = \frac{d}{da}\left(\int_a^\infty \frac{dx}{Dp_2(x)}\left[\int_x^\infty p_2(y)dy\right]^2\right) \tag{E5}$$

$$= \frac{-1}{Dp_2(a)} + \int_a^\infty dx\left[\frac{d}{da}\left(\frac{1}{Dp_2(x)}\right)\left[\int_x^\infty p_2(y)dy\right]^2 + \left(\frac{1}{Dp_2(x)}\right)\frac{d}{da}\left[\int_x^\infty p_2(y)dy\right]^2\right] \tag{E6}$$

$$= \frac{-1}{Dp_2(a)} + \int_a^\infty dx\left[\frac{-e^{-\beta v(a)}}{De^{-\beta v(x)}}\left[\int_x^\infty p_2(y)dy\right]^2 + \frac{2}{Dp_2(x)}\frac{e^{-\beta v(a)}}{\int_a^\infty e^{-\beta v(x)}dx}\left[\int_x^\infty p_2(y)dy\right]^2\right] \tag{E7}$$

$$= \frac{-1}{Dp_2(a)} - p_2(a)t_{a2} + 2p_2(a)t_{a2} = \frac{-1}{Dp_2(a)} + p_2(a)t_{a2}. \tag{E8}$$

Similarly, for the mean first passage time from the other side of the boundary

$$\frac{dt_{a1}}{da} = \frac{1}{Dp_1(a)} - p_1(a)t_{a1}. \tag{E9}$$

Substituting all these into Eq. (E1) and simplifying, it is found that the relaxation time is maximized at the condition

$$p_2(a)t_{a2} = p_1(a)t_{a1}, \tag{E10}$$

or equivalently

$$p_1^{eq} t_{a2} = p_2^{eq} t_{a1}. \tag{E11}$$

APPENDIX F: DERIVATION OF EQ. (46)

By increasing the number of clustered states to three, the number of free parameters in the correlation matrix grows from one to three. To limit the number of parameters, the potential $v(x)$ of the unclustered system is assumed to be symmetric. This has the effect of reducing the problem of finding two boundaries to just one boundary (at $-a$ and a). In this case, the relation between the relaxation time and the elements of the correlation matrix is given by (45). Writing the correlation matrix elements explicitly

$$\tau_2(a) = \frac{1}{p_1^{eq}}\left(2\int_0^\infty \frac{\langle\delta\theta_1(0)\delta\theta_1(t)\rangle}{\langle\delta\theta_1(0)^2\rangle}dt + \int_0^\infty \frac{\langle\delta\theta_1(0)\delta\theta_1(t)\rangle}{\langle\delta\theta_1(0)^2\rangle}dt\right) \tag{F1}$$

and using the same equations as in Appendix D to express them as integrals, one finds

$$\tau_2(a) = p_1^{eq}\int_{-a}^a \frac{dx}{Dp(x)}\left[\int_x^\infty p(y)dy\right] + \int_{-\infty}^{-a}\frac{dx}{Dp_1(x)}\left[\int_{-\infty}^x p_1(y)dy\right]^2. \tag{F2}$$

Similar to the previous case, these integrals can be related to mean first passage time quantities as

$$\tau_2(a) = p_1^{eq} t_{-aa} + t_{-a1}. \tag{F3}$$

REFERENCES

[1] S. Kube and M. Weber, J. Chem. Phys. **126**, 024103 (2007).
[2] F. Noé, I. Horenko, C. Schütte, and J. C. Smith, J. Chem. Phys. **126**, 155102 (2007).
[3] J. D. Chodera, N. Singhal, V. S. Pande, K. A. Dill, and W. C. Swope, J. Chem. Phys. **126**, 155101 (2007).
[4] D. Bicout and A. Szabo, Protein Sci. **9**, 452 (2000).
[5] N.-V. Buchete and G. Hummer, J. Phys. Chem. B **112**, 6057 (2008).
[6] V. S. Pande, K. Beauchamp, and G. R. Bowman, Methods **52**, 99 (2010).
[7] G. R. Bowman, V. S. Pande, and F. Noé, *An Introduction to Markov State Models and Their Application to Long Timescale Molecular Simulation* (Springer Netherlands, 2014).
[8] B. E. Husic and V. S. Pande, J. Am. Chem. Soc. **140**, 2386 (2018).
[9] C. Wehmeyer, M. K. Scherer, T. Hempel, B. E. Husic, S. Olsson, and F. Noé, Living J. Comput. Mol. Sci. **1**, 5965 (2018); available at https://www.livecomsjournal.org/article/5965-introduction-to-markov-state-modeling-with-the-pyemma-software-article-v1-0.
[10] H. Grubmüller and P. Tavan, J. Chem. Phys. **101**, 5047 (1994).
[11] M. I. Zimmerman, K. M. Hart, C. A. Sibbald, T. E. Frederick, J. R. Jimah, C. R. Knoverek, N. H. Tolia, and G. R. Bowman, ACS Cent. Sci. **3**, 1311 (2017).

[12]M. P. Harrigan, K. A. McKiernan, V. Shanmugasundaram, R. A. Denny, and V. S. Pande, Sci. Rep. **7**, 632 (2017).
[13]C. J. Dickson, V. Hornak, R. A. Pearlstein, and J. S. Duca, J. Am. Chem. Soc. **139**, 442 (2017).
[14]A. Kells, A. Annibale, and E. Rosta, J. Chem. Phys. **149**, 072324 (2018).
[15]K. M. Thayer, B. Lakhani, and D. L. Beveridge, J. Phys. Chem. B **121**, 5509 (2017).
[16]A. Bujotzek and M. Weber, J. Bioinf. Comput. Biol. **07**, 811 (2009).
[17]S. Doerr and G. De Fabritiis, J. Chem. Theory Comput. **10**, 2064 (2014).
[18]M. Badaoui, A. Kells, C. Molteni, C. J. Dickson, V. Hornak, and E. Rosta, J. Phys. Chem. B **122**, 11571 (2018).
[19]C. T. Leahy, A. Kells, G. Hummer, N.-V. Buchete, and E. Rosta, J. Chem. Phys. **147**, 152725 (2017).
[20]H. Wu and F. Noé, Multiscale Model. Simul. **12**, 25 (2014).
[21]E. Rosta and G. Hummer, J. Chem. Theory Comput. **11**, 276 (2014).
[22]L. S. Stelzl, A. Kells, E. Rosta, and G. Hummer, J. Chem. Theory Comput. **13**, 6328 (2017).
[23]G. R. Bowman, X. Huang, and V. S. Pande, Methods **49**, 197 (2009).
[24]L. Martini, A. Kells, R. Covino, G. Hummer, N.-V. Buchete, and E. Rosta, Phys. Rev. X **7**, 031060 (2017).
[25]R. Zwanzig, J. Stat. Phys. **30**, 255 (1983).
[26]P. Deuflhard, W. Huisinga, A. Fischer, and C. Schütte, Linear Algebra Appl. **315**, 39 (2000).
[27]M. Weber and K. Fackeldey, "G-PCCA: Spectral clustering for non-reversible Markov chains," Technical Report No. 15-35, ZIB, Takustr. 7, Berlin, 2015.
[28]S. Röblitz and M. Weber, Adv. Data Anal. Classif. **7**, 147 (2013).
[29]P. Deuflhard and M. Weber, Linear Algebra Appl. **398**, 161 (2005).
[30]M. Weber, "Clustering by using a simplex structure," Technical Report No. 04-03, ZIB, Takustr. 7, Berlin, 2003.
[31]M. Weber, "Improved Perron cluster analysis," Technical Report No. 03-04, ZIB, Takustr. 7, Berlin, 2003)
[32]Y. Yao, R. Z. Cui, G. R. Bowman, D.-A. Silva, J. Sun, and X. Huang, J. Chem. Phys. **138**, 174106 (2013).
[33]I. Horenko, E. Dittmer, A. Fischer, and C. Schütte, Multiscale Model. Simul. **5**, 802 (2006).
[34]V. Schultheis, T. Hirschberger, H. Carstens, and P. Tavan, J. Chem. Theory Comput. **1**, 515 (2005).
[35]G. R. Bowman, J. Chem. Phys. **137**, 134111 (2012).
[36]W. Wang, T. Liang, F. K. Sheong, X. Fan, and X. Huang, J. Chem. Phys. **149**, 072337 (2018).
[37]A. Jain and G. Stock, J. Chem. Theory Comput. **8**, 3810 (2012).
[38]A. Jain and G. Stock, J. Phys. Chem. B **118**, 7750 (2014).
[39]G. Hummer and A. Szabo, J. Phys. Chem. B **119**, 9029 (2014).
[40]C. Schütte and W. Huisinga, *Biomolecular Conformations can be Identified as Metastable Sets of Molecular Dynamics* (Elsevier, 2003).
[41]N. Djurdjevac, M. Sarich, and C. Schütte, Multiscale Model. Simul. **10**, 61 (2012).
[42]J.-H. Prinz, H. Wu, M. Sarich, B. Keller, M. Senne, M. Held, J. D. Chodera, C. Schütte, and F. Noé, J. Chem. Phys. **134**, 174105 (2011).
[43]F. P. Casey, J. J. Waterfall, R. N. Gutenkunst, C. R. Myers, and J. P. Sethna, Phys. Rev. E **78**, 046704 (2008).
[44]F. Noé and F. Nuske, Multiscale Model. Simul. **11**, 635 (2013).
[45]A. Berezhkovskii and A. Szabo, J. Chem. Phys. **121**, 9186 (2004).
[46]R. Zwanzig, Annu. Rev. Phys. Chem. **16**, 67 (1965).
[47]D. Chandler, J. Chem. Phys. **68**, 2959 (1978).
[48]A. Szabo, K. Schulten, and Z. Schulten, J. Chem. Phys. **72**, 4350 (1980).
[49]A. Perico, R. Pratolongo, K. F. Freed, R. W. Pastor, and A. Szabo, J. Chem. Phys. **98**, 564 (1993).
[50]D. Bicout and A. Szabo, J. Chem. Phys. **106**, 10292 (1997).
[51]J. L. Skinner and P. G. Wolynes, J. Chem. Phys. **69**, 2143 (1978).
[52]A. Berezhkovskii and A. Szabo, J. Chem. Phys. **122**, 014503 (2005).
[53]S. H. Northrup and J. T. Hynes, J. Chem. Phys. **69**, 5246 (1978).
[54]C. H. Jensen, D. Nerukh, and R. C. Glen, AIP Conf. Proc. **940**, 150–157 (2007).
[55]C. D. Meyer, Jr., Linear Algebra Appl. **22**, 41 (1978).
[56]J. C. Phillips, R. Braun, W. Wang, J. Gumbart, E. Tajkhorshid, E. Villa, C. Chipot, R. D. Skeel, L. Kale, and K. Schulten, J. Comput. Chem. **26**, 1781–1802 (2005).